Quantum-Computing-Inspired Probabilistic Power Flow Calculation in Renewable-Rich Systems

Zhen Xu
College of EE
Zhejiang University
Hangzhou, China
zhen_xu@zju.edu.cn

Zhiyi Li*
College of EE
Zhejiang University
Hangzhou, China
zhiyi@zju.edu.cn

Xutao Han
College of EE
Zhejiang University
Hangzhou, China
xutao_han@zju.edu.cn

Yue Xu
College of EE
Zhejiang University
Hangzhou, China
yue_xu@zju.edu.cn

***Abstract*—The paper proposes a Quantum Probabilistic Power Flow (QPPF) algorithm to achieve high-precision estimation of voltage fluctuation and power flow distribution in renewable-rich systems with reduced quantum hardware. Addressing the complexity arising from high-dimensional statistical moments, we propose a quantum-enhanced Three-Point Estimate Method. This method achieves a quadratic speedup in the convergence of statistical moment errors for renewable energy output, thereby ensuring the accurate representation of statistical discretization. With the dramatic increase in power flow analyses required by discretized scenarios, we introduce a quantum parallel power flow framework. By multiplexing power flow solutions into a quantum circuit, it minimizes quantum processing unit calls and hardware demands, while performing high-precision calculation across power flows of varying scales in constant time, thereby evaluating voltage and power flow distributions. Finally, we employ the modified IEEE-14 and 3 systems to verify the feasibility, accuracy and efficiency of the QPPF algorithm.**

***Index Terms*—probabilistic power flow, point estimated method, quantum computing, quantum power flow, renewable energy**

I. INTRODUCTION

The increasing penetration of renewable energy sources, such as wind and photovoltaic (PV), introduces significant stochasticity and volatility into the system [1], shifting the system's operational paradigm from deterministic to stochastic and imparting probabilistic characteristics to system state variables, i.e., voltages and power flows. Probabilistic Power Flow (PPF) has emerged as an essential tool for quantifying the impact of these uncertainties on the system's operational state. By analyzing the statistical characteristics of the system state variables, PPF is employed to assess potential operational risks, such as voltage violations and power flow congestion. However, in renewable-rich systems, the high dimensionality of stochastic input variables causes the statistical analysis required by PPF to inevitably face the curse of dimensionality.

Classical PPF can be classified as approximate, analytical, and simulation-based methods. Among these, the Three-Point Estimation Method (3PEM), a type of approximate method, uses statistical moments to discretize continuous probability distributions into a limited set of power flow scenarios [2]. The 3PEM offers a significant advantage by simultaneously avoiding the extensive sampling burden of simulation methods and the accuracy loss from linearization common in analytical methods. However, the estimation accuracy of 3PEM relies on high-precision statistical moments, the calculation of which requires large-scale sampling or high-dimensional integration [3]. In renewable-rich systems, the high dimensionality of stochastic input variables renders the calculation of statistical moments computationally prohibitive. Fortunately, with the principles of quantum computing [4], Quantum Monte Carlo (QMC) simulation, designed for the accurate estimation of expected values, reduces the computational complexity from $O(1/\varepsilon^2)$ to $O(1/\varepsilon)$ relative to classical Monte Carlo (CMC) [5]. That is, QMC utilizes fewer quantum queries to estimate raw moments with precision comparable to that of CMC, serving as a basis for the high-precision derivation of central moments. While the superiority of QMC has been demonstrated in other fields [6], its potential for estimating high-dimensional statistical moments in PPF analysis remains unexplored.

Another critical challenge is that numerous input variables cause a surge in the power flow scenarios. Although the required calculation is typically less than that of simulation-based methods, the dimension-dependent characteristic causes the efficiency advantage of 3PEM to diminish significantly. Existing quantum solutions [7], termed Quantum Power Flow (QPF), employ the HHL algorithm to calculate the correction equation, promising an exponential reduction in computational complexity on quantum computers. However, a key limitation is that QPF algorithms solve only a single correction equation within a single quantum circuit. The requirement to solve multiple equations entails repetitive circuit reconstruction and frequent queuing for cloud-based quantum access [8]. These resource-intensive processes may introduce significant latency, creating an additional efficiency bottleneck for PPF analysis. Consequently, storing power flow equations in quantum superposition and processing correction vectors in parallel via a single quantum circuit are crucial for ensuring the PPF's computational advantage in renewable-rich systems, while minimizing quantum resource requirements.

To this end, we propose a Quantum PPF (QPPF) method to enhance both the accuracy of system state estimation and overall computational efficiency, while reducing required quantum resources. The main contributions are as follows:

1) We introduce a quantum-enhanced 3PEM to achieve a quadratic speedup in statistical moment estimation, ensuring accurate statistical discretization.

2) We propose a quantum parallel power flow framework to evaluate system state, achieving constant time and reduced quantum hardware under discrete scenarios of varying scales.

3) We illustrate the advantages of the proposed algorithm mathematically, and validate them by numerical simulation.

This work was supported by the National Natural Science Foundation of China under Grant 52477132.

979-8-3315-8138-1

II. QUANTUM PROBABILISTIC POWER FLOW ALGORITHM

A. PPF Calculation Principles for Renewable-Rich Systems

The stochasticity of power systems mainly stems from the fluctuations of wind and PV power, as considered in this paper. To evaluate the impact of these uncertainties on power flow and voltage distributions, the classical 3PEM operates by leveraging the statistical moments of the input variables to generate discrete scenarios and corresponding weights. This process transforms the PPF problem into a limited number of deterministic power flow calculations, whose results are then synthesized through a weighted sum to accurately yield the statistical moments of the output variables. Motivated by the numerous uncertainties in renewable-rich systems, a QPPF algorithm is proposed and illustrated in Fig. 1, which provides a quantum solution for the escalating computational burden of the high-dimensional statistical moment estimation and power flow calculations. Principal steps are illustrated as:

1) **Step 1**: The probability distribution and its power function are encoded into the quantum circuit using the operations $\boldsymbol{T}_0$ and $\boldsymbol{T}_1$ so as to estimate the value $E[\boldsymbol{P}]$.

2) **Step 2**: The Grover operator $\boldsymbol{G}$ is designed and operated to quadratically accelerate the estimation of $E[\boldsymbol{P}]$ in accordance with Quantum Amplitude Estimation (QAE).

3) **Step 3**: The expected values (i.e., raw moments) are used to calculate the central moments using the 3PEM. Then, the discrete scenarios are generated for QPF calculations.

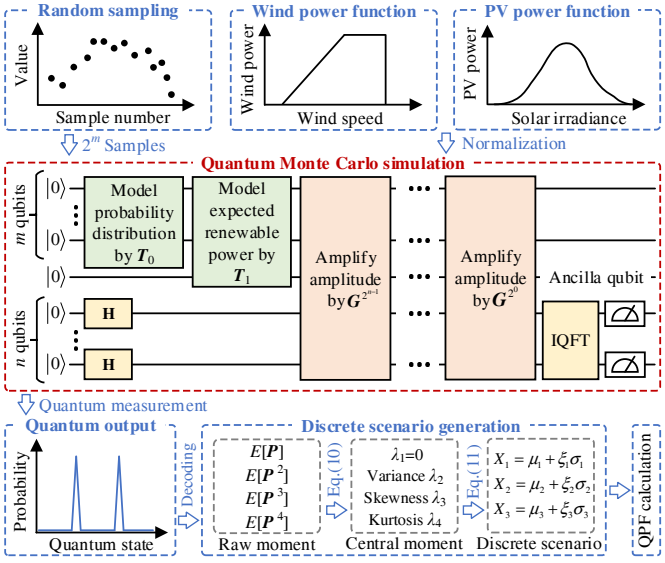

Fig. 1. Schematic diagram of QPPF algorithm.

B. Problem Mapping of Statistical Moment Estimation

The process begins by discretizing the continuous variable (e.g., wind speed and solar irradiances, characterized by the Weibull and Beta distributions respectively) into 2^m samples. These samples are then mapped onto the 2^m basis states of an m-qubit register. An operation $\boldsymbol{T}_0$ is applied to the m-qubit register to load the distribution, resulting in the quantum state, which is illustrated in (1). This process encodes the uniform probability distribution into the quantum state.

$$|\psi\rangle = \sum_{i=0}^{2^m-1} \sqrt{p_i}\,|i\rangle \tag{1}$$

where $|\psi\rangle$ is the state of the quantum system; $|i\rangle$ and $\sqrt{p_i}$ are the basis state and its corresponding probability amplitude.

The power function P_i is normalized and encoded onto an ancilla qubit via the oracle operation $\boldsymbol{T}_1$, shown in (2). This operation maps the normalized values P_i' to the amplitude of the ancilla qubit. As a result (3), the normalized expected value is precisely equal to the probability of measuring the ancilla in the $|1\rangle$ state. However, to achieve a target error ε, a naive estimation based on repeating (2) and measurement 2^m times requires a query complexity of $O(1/\varepsilon^2)$. The QAE algorithm can overcome the issue.

$$\boldsymbol{T}_1\boldsymbol{T}_0\,|0\rangle^{\otimes(m+1)} = \sum_{i=0}^{2^m-1} \sqrt{p_i}\,|i\rangle\left(\sqrt{1-P_i'}\,|0\rangle + \sqrt{P_i'}\,|1\rangle\right) \tag{2}$$

$$p_{\mathrm{a}} = \sum_{i=0}^{2^m-1} p_i P_i' \approx E[\boldsymbol{P}]/P_{\mathrm{r}} \tag{3}$$

C. Quantum-Enhanced Statistical Moment Estimation

Using the Quantum Phase Estimation framework and the Grover operator $\boldsymbol{G}$, the QAE provides a potential quadratic speedup for the expected value estimation. As a preliminary step, equation (2) is written as (4). The Grover operator $\boldsymbol{G}$ is formulated based on operations $f_0 = (I - 2|0\rangle\langle 0|^{\otimes(m+1)})$ and $f_1 = (I - 2|\psi_1\rangle\langle\psi_1|)$, as given by (5), which clearly reveals the geometric essence of $\boldsymbol{G}$: it performs a deterministic rotation by an angle of 2θ within the two-dimensional subspace spanned by $|\psi\rangle$ and $|\psi_1\rangle$. The QAE algorithm employs a total of $m + n$ qubits to estimate ϕ as an n-bit binary string $\phi_1\phi_2\ldots\phi_n$ by applying a sequence of powered Grover operators. The value $E[\boldsymbol{P}]$ can be calculated using (6).

$$\boldsymbol{T}_1\boldsymbol{T}_0\,|0\rangle^{\otimes(m+1)} = \boldsymbol{T}\,|0\rangle^{\otimes(m+1)} = |\psi\rangle = \cos(\theta)|\psi_0\rangle + \sin(\theta)|\psi_1\rangle \tag{4}$$

$$\boldsymbol{G} = -\boldsymbol{T}f_0\boldsymbol{T}^{-1}f_1 = -\left(\boldsymbol{I} - 2|\psi\rangle\langle\psi|\right)\left(\boldsymbol{I} - 2|\psi_1\rangle\langle\psi_1|\right) \tag{5}$$

$$E[\boldsymbol{P}] \approx \sin^2\left[\pi\left(\frac{\phi_1}{2^1} + \frac{\phi_2}{2^2} + \ldots + \frac{\phi_n}{2^n}\right)\right] P_{\mathrm{r}} \tag{6}$$

where $|\psi_0\rangle$ and $|\psi_1\rangle$ separately denote the states where the ancilla qubit is measured as $|0\rangle$ and $|1\rangle$; $\theta = \arcsin(\sqrt{p_{\mathrm{a}}}) = \pi\phi$; $\boldsymbol{I}$ is the identity operator; P_{r} is the rated power.

The QAE introduces an approximation error for p_{a}, arising from using a finite n-qubit register to estimate the continuous phase ϕ. The complexity to achieve an estimation error ε scales as $O(1/\varepsilon)$, demonstrating a quadratic speedup over CMC [6], providing essential support for the high-precision calculation of central moments.

D. Generation of Discrete Power Flow Scenarios

For the input uncertainties $\boldsymbol{X}_t$, the discrete scenarios for PPF analysis can be formulated as (7). The raw moments of $\boldsymbol{X}_t$, estimated using the methods in Sections II-B and II-C, are used to compute the standardized moments $\lambda_{t,z}$ and weights $q_{t,r}$ based on (8)-(9). Finally, the raw moment of the output function can be calculated using (10) by performing deterministic power flow calculations for each scenario $X_{t,r}$. With the high-precision estimation of central moments, the PPF can be effectively applied to renewable-rich systems.

$$X_{t,r} = \mu_t + \xi_{t,r}\sigma_t \quad r = 1,2,\cdots,R,\ t = 1,2,\cdots,T \tag{7}$$

$$\lambda_{t,z} = E\left[\left(\boldsymbol{X}_t - E[\boldsymbol{X}_t]\right)^z\right] \Big/ (\sigma_t)^z \quad z = 1,2,\cdots \tag{8}$$

$$\sum_{r=1}^{R} q_{t,r}\left(\xi_{t,r}\right)^{z} = \lambda_{t,z} \tag{9}$$

$$E\left[F\left(X\right)^{z}\right] = \sum_{t=1}^{T}\sum_{r=1}^{R} q_{t,r}\left[f\left(\mu_1,\ldots,X_{t,r},\ldots,\mu_T\right)\right]^{z} \tag{10}$$

where $\lambda_{t,z}$, μ_t, $\xi_{t,r}$ and σ_t represent the standardized central moment, mean, location and standard deviation, respectively.

III. Parallel Implementation for QPPF Algorithm

A. Quantum Power Flow under Discrete Scenarios

The power flow equations of each discrete scenario can be formulated as (11)-(12), which are solved to quantify the effects of uncertain variables from renewable energy sources on voltage violation and power flow distribution. As detailed in [9], these equations with the linear form $\boldsymbol{Ax} = \boldsymbol{b}$ can be solved with HHL algorithm, as illustrated in Fig. 2, offering an exponential speedup over the conjugate gradient method.

$$\Delta \boldsymbol{P}/\boldsymbol{V}^2 = -\boldsymbol{B}'\Delta\boldsymbol{\delta} \tag{11}$$

$$\Delta \boldsymbol{Q}/\boldsymbol{V}^2 = -\boldsymbol{B}''\Delta\boldsymbol{V} \tag{12}$$

where $\Delta\boldsymbol{P}$ and $\Delta\boldsymbol{Q}$ are imbalance vectors; $\Delta\boldsymbol{V}$ and $\Delta\boldsymbol{\delta}$ are correction vectors; $\boldsymbol{V}$ is voltage magnitude; $\boldsymbol{B}'$ and $\boldsymbol{B}''$ are constant matrices.

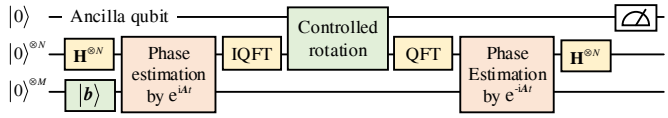

Fig. 2. QPF calculation based on the HHL algorithm.

However, the numerous input variables of renewable-rich systems cause a surge in power flow equations, as detailed in (7)-(10). Applying the HHL algorithm sequentially to each scenario necessitates repetitive circuit reconstruction and task queuing for cloud-based quantum device access. This process introduces a significant additional bottleneck, effectively mitigating the theoretical advantage of HHL when scaled to the complete PPF analysis. Then, we propose a quantum parallel power flow framework to address the challenge.

B. Quantum Parallel Power Flow Framework

The fidelity of the HHL algorithm is primarily determined by the size of the N-qubit register [10]. On the one hand, N must be large enough to provide sufficient resolution for the phases corresponding to the rescaled eigenvalues of matrix $\boldsymbol{A}$, where the necessary rescaling is determined by the spectral radius. On the other hand, N must provide sufficient phase estimation precision for small eigenvalues. This is essential to prevent the controlled-rotation, dependent on the eigenvalue, $1/\lambda_j$, from amplifying errors. Therefore, for linear equations whose matrices share identical spectral properties, N is the same, regardless of their dimensions.

As for the correction equation $\Delta\boldsymbol{P}_{t,r}/\boldsymbol{V}_{t,r}^2 = -\boldsymbol{B}'\Delta\boldsymbol{\delta}_{t,r}$ of $X_{t,r}$, a key feature is that the matrix $\boldsymbol{B}'$ and its spectral properties remain constant. Leveraging this uniformity, the equations can be expanded as formulated in (13) and then solved in parallel through a single execution of HHL; and the quantum phase estimation employs the same unitary operator $U=e^{iAt}$ in parallel. The amplitude of the (t, r)-th solution component in this superposition is proportional to the relative norm $\|\boldsymbol{b}_{t,r}\|/\|\boldsymbol{b}'\|$ requiring a classical rescaling step to recover the actual numerical values from the measured quantum state. This parallel formulation increases the problem's dimensionality without changing the spectral properties (e.g., the condition number κ and the sparsity s) strategically. Therefore, the number of qubits M increases to encode the larger equation, but the number of qubits N does not need to change to maintain the same level of fidelity ς.

$$\underbrace{-\begin{bmatrix}\boldsymbol{B}' & & \\ & \ddots & \\ & & \boldsymbol{B}'\end{bmatrix}}_{A'}\underbrace{\begin{bmatrix}\Delta\boldsymbol{\delta}_{1,1}\\ \vdots \\ \Delta\boldsymbol{\delta}_{T,R}\end{bmatrix}}_{x'} = \underbrace{\begin{bmatrix}\Delta\boldsymbol{P}_{1,1}/\boldsymbol{V}_{1,1}^2\\ \vdots \\ \Delta\boldsymbol{P}_{T,R}/\boldsymbol{V}_{T,R}^2\end{bmatrix}}_{b'} \tag{13}$$

The contributions of the proposed method are as follows: 1) It introduces a novel quantum parallel power flow framework, as compared with its classical counterpart in Fig. 3. While the classical framework distributes tasks across multiple processors to accelerate the solution of individual problems, the proposed framework aggregates multiple power flow tasks and processes them on a single quantum circuit using the HHL algorithm. 2) The number of required qubits is reduced from approximately TR·(N + M + 1) to (N + M + 1 + log(TR)), with the quantum gate count reduced by a comparable ratio. 3) The number of QPU calls is reduced from TR to 1. 4) The time complexity is lowered from $TR{\cdot}O(\log(2^M){\cdot}s^2{\cdot}\kappa^2{\cdot}\varsigma^{-1})$ to $O((\log(TR)+\log(2^M)){\cdot}s^2{\cdot}\kappa^2{\cdot}\varsigma^{-1})$. This approach is suitable for the equation $\Delta\boldsymbol{Q}_{t,r}/\boldsymbol{V}_{t,r}^2 = -\boldsymbol{B}''\Delta\boldsymbol{V}_{t,r}$.

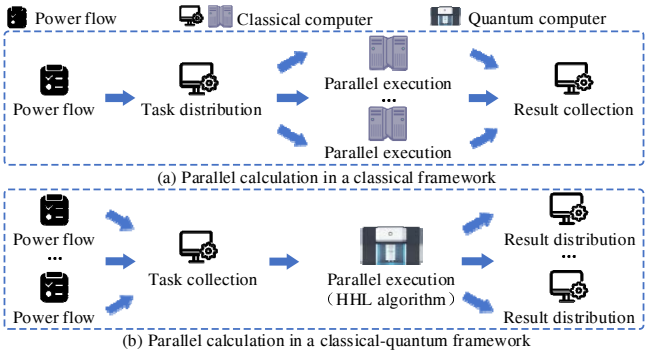

Fig. 3. Schematic diagram of quantum parallel power flow framework.

C. Overview of Quantum-Oriented Implementation Steps

The overview of the QPPF algorithm for renewable-rich systems are shown in Algorithm 1, where QPU and CPU are coordinated according to Fig. 1 and Fig. 3. Detailed steps are:

Algorithm 1: Quantum Probabilistic Power Flow

Input: Random power samples and uniform probability;
  Calculate $E[\boldsymbol{P}]$, $E[\boldsymbol{P}^2]$, $E[\boldsymbol{P}^3]$ and $E[\boldsymbol{P}^4]$ using QMC;
  Generate discrete scenarios using (7)-(9);
  Construct power flow equation using (11)-(13);
  if $\max(\Delta\boldsymbol{\delta}) \geq 10^{-6}$ **&&** $\max(\Delta\boldsymbol{V}) \geq 10^{-6}$ **then**
    Solve (13) using HHL algorithm;
    Update bus voltages;
  else
    Calculate the statistical information based on (10);
  end if
Output: Voltage and power flow distribution.

1) **Step 1**: Generate discrete scenarios based on the quantum-enhanced 3PEM. By repeatedly executing the procedures described in Sections II-B and II-C, the expected

values are obtained via the QMC algorithm. Subsequently, $X_{t,r}$ and $q_{t,r}$ are calculated based on (7)-(9).

2) **Step 2**: Construct the superposition of multiple power flows. The deterministic power flow equations are formulated using (11)-(12), and the corresponding superposition equation for the $\boldsymbol{B}'$ or $\boldsymbol{B}''$ matrices is generated respectively using (13), to be solved via the HHL algorithm.

3) **Step 3**: Analysis of voltage fluctuation and power flow distribution. The statistical moments of the output variables are synthesized based on (10) and the HHL solution results. Then, the impact of renewable energy sources on system voltage fluctuation and power flow distribution is evaluated.

IV. Numerical Results

Numerical experiments are conducted on the IEEE 14-bus system by integrating 20 MW wind farms at buses 3, 4, 9, and 13, and a 25 MW PV farm at bus 14. The values $E[\boldsymbol{P}]$ of the wind farm and the photovoltaic farm are separately calculated as 7.93 MW and 16.35 MW. The renewable penetration level is set to an average of approximately 15% of the total system load, peaking at around 40%. The hardware configuration used to run the ideal quantum simulator consisted of an Intel Core i5-14400 processor with 16 GB of RAM.

Through repeated experiments of the 20 MW wind farm, the estimation error between QMC and CMC is compared under an equivalent number of sample running. The results of both algorithms converge on the theoretical value 7.93 MW. As shown in Fig. 4, with a 2^8-fold increase in the number of sampling runs, the estimation error of the CMC simulation decreases from 0.84 to 5.06×10^{-2}, aligning perfectly with the theoretical convergence rate $O(1/\varepsilon^2)$. In contrast, the error of QMC decreases from 2.94×10^{-2} to 1.20×10^{-6}, which matches or even exceeds the theoretical rate $O(1/\varepsilon)$. QMC achieves a quadratic acceleration in the estimation error convergence of expected value, yielding a lower error under same number of quantum queries. Notably, when the number of quantum queries reaches 2^{11}, the estimation error of QMC is entirely below its theoretical upper bound of 4.88×10^{-4}, which makes $n = 11$ as a robust parameter for QPPF analysis.

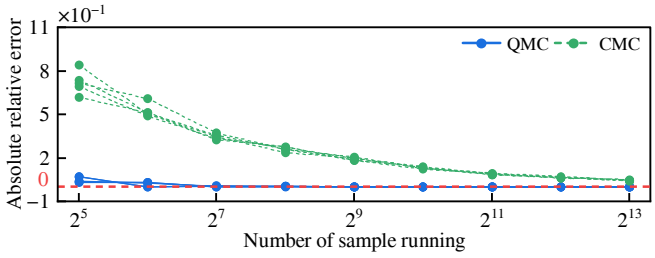

Fig. 4. Comparison of convergence rates of QMC and CMC.

For the variables following Weibull and Beta distributions, the raw moments derived from the quantum-enhanced 3PEM exhibit high consistency with theoretical values, with computational errors for all orders suppressed to 10^{-4} or below. As illustrated in Fig. 4, the error scaling of QMC maintains $1/\sqrt{2^m}$ regardless of the moment's dimensionality. In contrast, for conventional methods such as trapezoidal integration, the convergence rate deteriorates as dimensionality increases under a fixed sample size. This confirms the efficacy of QMC in substituting high-dimensional integration for moment calculation, ensuring the precise generation of representative scenarios in (7) and the reliability of QPPF calculations in power systems with high renewable energy penetration.

In accordance with Section II-D, 11 deterministic power flow scenarios are derived from the discrete scenarios. To solve (11) for each individual scenario, the HHL algorithm requires $N = 11$ and $M = 4$ qubits per execution. When solving 11 scenarios in parallel as shown in Fig. 3(b), the eigenvalues in (13) remain consistent with those in (11). However, while N remains 11, the required number of qubits M increases to 8 to accommodate the storage of the expanded eigenvectors. This qubit configuration is equally applicable to the solution of (12). The power flows are solved using both the sequential mode and the quantum parallel mode, while Table I shows the required quantum hardware. Fig. 5 illustrates that the results of the parallel model are consistent with the classical method. The parallel mode achieves a significant hardware saving, reducing the quantum gate count by 90.50%, qubit count by 88.82% and the number of QPU calls by 90.83%. The results of the parallel model are consistent with the classical power flow method. These reductions confirm the advantages described in Section III-B.

TABLE I. Comparison of Required Quantum Hardware

	Qubit	Quantum gate	QPU calls
[9]	17792	7.05×10^6	1112
Fig. 3 (b)	1988	6.69×10^5	102

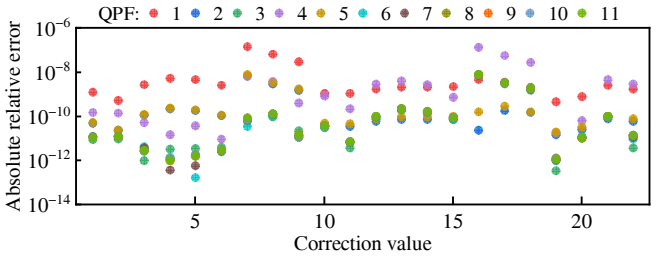

Fig. 5. Calculation error of the quantum parallel power flow.

Fig. 6 illustrates the quantum resources and computational time required to solve power flow scenarios across different group sizes. The number of quantum gates and qubits increased by 3.15% and 14.71%, respectively. Leveraging the superposition state of M-qubit registers, the qubit requirement remains invariant when solving varying numbers of power flow problems, with the time stabilizing at approximately 0.90 s (e.g., at a 37-qubit scale). This stability is further validated at scales of 38 and 39 qubits. It should be noted that the quantum simulator time is relatively long and is influenced by the classical hardware configuration. Overall, taking (11) as an example, which contains a matrix of dimension 13, the increase in the M-qubit register capacity enables the solution of (13) containing $2^{M-1}/13$ to $2^M/13$ equations in constant time. Consequently, addressing the explosive growth of computational demand in renewable-rich power systems, the parallel method provides a quantum-perspective solution for constant-time power flow analysis.

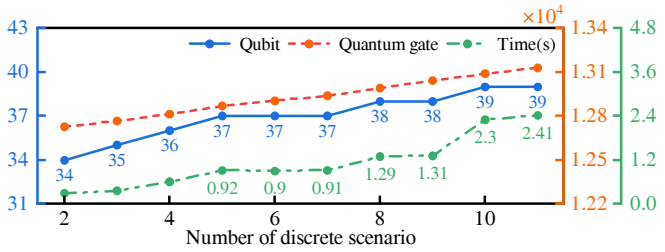

Fig. 6. Computation overhead of the quantum parallel method.

Fig. 7 illustrates the voltage mean and standard deviation for PQ buses. Voltage violations are observed at the majority of PQ nodes. Bus 14, in particularly, stands out as the most unstable point; its integrated 25 MW PV farm far surpasses its native load, causing severe voltage variations from 1.044 to 1.060 p.u. as it oscillates between net-load and net-generation states. Wind power injections at the neighboring Buses 9 and 13 create a regional high-voltage pocket (including Buses 7, 9, 10, 13, and 14). Reflecting the fluctuations of input variables, the reverse power flow probabilities for branches 4-5, 3-4, 10-11, and 12-13 reach 100%, exhibiting a distinct outward transmission characteristic. Furthermore, branches 7-8 and 9-14 present reverse probabilities of 69.1% and 59.3%, respectively, reflecting high uncertainty in power flow directions. The low-impedance Branch 1-2 absorbs major imbalances from Bus 3 and Bus 4, causing its flow to range from 115.81 MW to 128.80 MW and resulting in a 100% congestion probability. The above issues can be mitigated by reducing the voltage set-points at Bus 6 and Bus 8, and by upgrading the capacity of Branch 1-2.

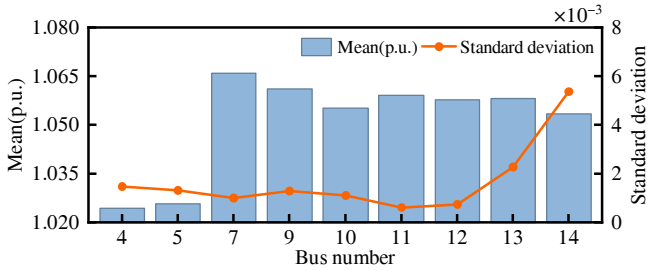

Fig. 7. Voltage mean and standard deviation of PQ buses.

The IEEE 3-bus system with the topology shown in [8] is utilized to verify the performance of the proposed algorithm on Origin Quantum's noisy superconducting quantum computer, with a wind variable incorporated into the model. A total of 3 representative scenarios and 6 power flow equations are generated. Notably, the eigenvalues of (11) and (12) are both 1 and 2, implying that 6 power flow equations can be solved via a single HHL execution. Due to the excessive number of quantum gates required by the QMC under the n = 11, the proposed parallel computing mode is verified on the quantum computer, with the quantum circuit design referencing [10]. By streamlining processes such as task queuing and data transmission, the total quantum calculation time on the quantum computer is reduced from 1277.41s to 140.76s, improving efficiency by 88.98%, while maintaining results consistent with the classical method. Quantum hardware resource savings exceed 70% per single iteration. Furthermore, the parallel solving of power flow equations across different scales maintains a nearly constant execution time of 1.15-1.22s per iteration (excluding data transmission factors). From a quantum computing perspective, these results demonstrate that the proposed parallel computing mode can significantly conserve quantum resources and solve multiple power flow equations in constant time.

V. Conclusion

This paper proposes a QPPF algorithm for renewable-rich systems that leverages quantum computing to enhance both the accuracy of system state estimation and overall computational efficiency. To verify the algorithm, simulations are conducted on a noisy superconducting quantum computer and an ideal simulator. Based on the numerical results, the quantum-enhanced 3PEM achieves a quadratic speedup in the convergence of the estimation error, accurately estimates the central moments of renewable output, and precisely discretizes the input probability distributions. Furthermore, considering the 'curse of dimensionality' caused by numerous input stochastic variables, the quantum parallel mode for multiple power flows effectively mitigates the computational burden; it greatly reduces quantum hardware requirements while ensuring high-precision statistical results. The parallel execution paradigm substantially mitigates task latency by reducing task scheduling and minimizing cloud data transfer overhead. Constrained by current quantum hardware limitations, the scalability of this scheme to large-scale power systems and its experimental validation on quantum computers are left for future research.

References

[1] M. M. R. Ahmed *et al.*, "Mitigating Uncertainty Problems of Renewable Energy Resources Through Efficient Integration of Hybrid Solar PV/Wind Systems into Power Networks," *IEEE Access*, vol. 12, pp. 30311–30328, 2024.

[2] Y. Che, X. Chen, H. Lin, Y. Gao, X. Lyu, and Y. Chen, "Temporal Impact of High-Speed Railway Traction Load on Grid Voltage Considering the Uncertainty," *IEEE Trans. Transp. Electrific.*, vol. 10, no. 4, pp. 9381–9395, Dec. 2024.

[3] G. Sun, S. Chen, Z. Wei, and S. Chen, "Multi-period integrated natural gas and electric power system probabilistic optimal power flow incorporating power-to-gas units," *J. Mod. Power Syst. Clean Energy*, vol. 5, no. 3, pp. 412–423, May 2017.

[4] Y. Xu, X. Han, Z. Xu, and Z. Li, "Quantum Computing for Facilitating the Design and Operation of More Sustainable Power Systems: Achieving Superior Performance Beyond Classical Computing Through Quantum Properties," *IEEE Energy Sustain. Mag.*, vol. 1, no. 1, pp. 90–105, May 2025.

[5] X. Han, Z. Li, W. Gu, and M. Shahidehpour, "Quantum Computing for Stochastic Economic Dispatch in Renewables-Rich Power Systems," *IEEE Trans. Smart Grid*, vol. 16, no. 5, pp. 4113–4127, Sept. 2025.

[6] T. Matsakos and S. Nield, "Quantum Monte Carlo simulations for financial risk analytics: scenario generation for equity, rate, and credit risk factors," *Quantum*, vol. 8, 1306, Apr. 2024.

[7] Y. Zhou *et al.*, "Quantum computing in power systems," *iEnergy*, vol. 1, no. 2, pp. 170–187, June 2022.

[8] B. Sævarsson, S. Chatzivasileiadis, H. Jóhannsson, and J. Østergaard, "Quantum computing for power flow algorithms: Testing on real quantum computers," arXiv preprint arXiv:2204.14028, 2022.

[9] Feng, Y. Zhou and P. Zhang, "Quantum Power Flow," *IEEE Trans. Power Syst.*, vol. 36, no. 4, pp. 3810-3812, July 2021.

[10] A. W. Harrow, A. Hassidim, and S. Lloyd, "Quantum algorithm for linear systems of equations," Phys. Rev. Lett., vol. 103, no. 15, 150502, Oct. 2009.